Environmental Research Letters

LETTER

Drivers and patterns of land biosphere carbon balance reversal

Christoph Müller[1,4], Elke Stehfest[2], Jelle G van Minnen[2], Bart Strengers[2], Werner von Bloh[1], Arthur H W Beusen[2], Sibyll Schaphoff[1], Tom Kram[2] and Wolfgang Lucht[1,3]

[1] Potsdam Institute for Climate Impact Research, Telegraphenberg A31, D-14473 Potsdam, Germany
[2] PBL Netherlands Environmental Assessment Agency, 3720 AH, Bilthoven, The Netherlands
[3] Department of Geography, Humboldt Universität zu Berlin, D-10099 Berlin, Germany
[4] Author to whom any correspondence should be addressed.

E-mail: Christoph.Mueller@pik-potsdam.de

Abstract

The carbon balance of the land biosphere is the result of complex interactions between land, atmosphere and oceans, including climatic change, carbon dioxide fertilization and land-use change. While the land biosphere currently absorbs carbon dioxide from the atmosphere, this carbon balance might be reversed under climate and land-use change ('carbon balance reversal'). A carbon balance reversal would render climate mitigation much more difficult, as net negative emissions would be needed to even stabilize atmospheric carbon dioxide concentrations. We investigate the robustness of the land biosphere carbon sink under different socio-economic pathways by systematically varying climate sensitivity, spatial patterns of climate change and resulting land-use changes. For this, we employ a modelling framework designed to account for all relevant feedback mechanisms by coupling the integrated assessment model IMAGE with the process-based dynamic vegetation, hydrology and crop growth model LPJmL. We find that carbon balance reversal can occur under a broad range of forcings and is connected to changes in tree cover and soil carbon mainly in northern latitudes. These changes are largely a consequence of vegetation responses to varying climate and only partially of land-use change and the rate of climate change. Spatial patterns of climate change as deduced from different climate models, substantially determine how much pressure in terms of global warming and land-use change the land biosphere will tolerate before the carbon balance is reversed. A reversal of the land biosphere carbon balance can occur as early as 2030, although at very low probability, and should be considered in the design of so-called peak-and-decline strategies.

Introduction: the land biosphere carbon sink

The land biosphere presently absorbs substantial amounts of carbon dioxide (CO_2) from the atmosphere, partially compensating CO_2 emissions from fossil fuel combustion and land use change and thus slowing anthropogenic climate change. Over the last three decades, land surfaces have absorbed about 2.3 ± 0.8 Pg carbon (C) per year. Over the same period, land use change has led to average emissions of 1.0 ± 0.5 Pg C yr^{-1}, leaving a net carbon sink of 1.3 Pg C yr^{-1} (Le Quéré *et al* 2014). This net carbon flux from the atmosphere to the land biosphere is a prominent negative (dampening) feedback mechanism in the Earth system (Friedlingstein *et al* 2006) that slows the rate of increase of atmospheric CO_2. The inter-annual variability of the land–atmosphere carbon flux reflects its sensitivity to changes in precipitation in sensitive ecosystems (Schwalm *et al* 2012, Gatti *et al* 2014, Poulter *et al* 2014) as well as to variations in temperature (Lucht *et al* 2002). Land carbon uptake is projected to increase under climate change, mainly driven by the positive effects of CO_2 fertilization of photosynthesis (Sitch *et al* 2008, Friend *et al* 2014), which are subject to large uncertainties (Schimel *et al* 2015). However, under high emission scenarios and severe climate change, some studies have found that the

land–atmosphere carbon flux could decrease or even reverse direction (Schaphoff *et al* 2006, Scheffer *et al* 2006, Sitch *et al* 2008), converting the negative feedback (dampening the atmospheric CO_2 burden) into a positive feedback (increasing the atmospheric CO_2 burden) and thereby amplifying rather than decreasing anthropogenic climate change. The consequences of such a change in feedback sign (negative to positive) are qualitatively different from those of a mere decline in carbon sink strength: humankind would not only have to mitigate a larger fraction of its own emissions but would rather have to compensate additional CO_2 flows from the biosphere that are not as directly manageable. However, mechanisms and likelihood of such a reversal have not been clearly identified and critical levels of climate change for such carbon balance reversal of the land biosphere remain unclear.

The properties of feedback mechanisms between atmospheric CO_2 concentrations, climate and the land carbon balance (Arora *et al* 2013) as well as land-use patterns (Gasser and Ciais 2013, Pongratz *et al* 2013) determine the robustness of the terrestrial carbon sink. Human land management both alters land productivity and carbon stocks significantly (Haberl *et al* 2007, Müller *et al* 2007). Climate change will substantially affect natural ecosystems, but equally agricultural productivity (Rosenzweig *et al* 2014) and subsequently land-use patterns (Kicklighter *et al* 2014, Nelson *et al* 2014, Schmitz *et al* 2014). Studies on the robustness of the terrestrial carbon sink have typically focused on the response of the land biosphere to climate change only (Schaphoff *et al* 2006, Scheffer *et al* 2006, Sitch *et al* 2008).

We here investigate under what climatic and socio-economic conditions the land biosphere's carbon balance is reversed, i.e. under which circumstances it changes from a net carbon sink to a net carbon source. For this, we employ a novel integrated modelling framework by coupling the process-based dynamic global vegetation, hydrology and crop growth model LPJmL (Bondeau *et al* 2007) with the comprehensive integrated assessment model IMAGE2.4 (Bouwman *et al* 2006, Stehfest *et al* 2014). This setting allows for including all relevant feedback mechanisms between atmospheric CO_2 concentrations ([CO_2]), climate change, oceanic carbon uptake, land-use change and the land biosphere's carbon balance. As such, changing agricultural productivity under CO_2 fertilization and climate change directly affect land-use patterns and associated emissions from land-use change.
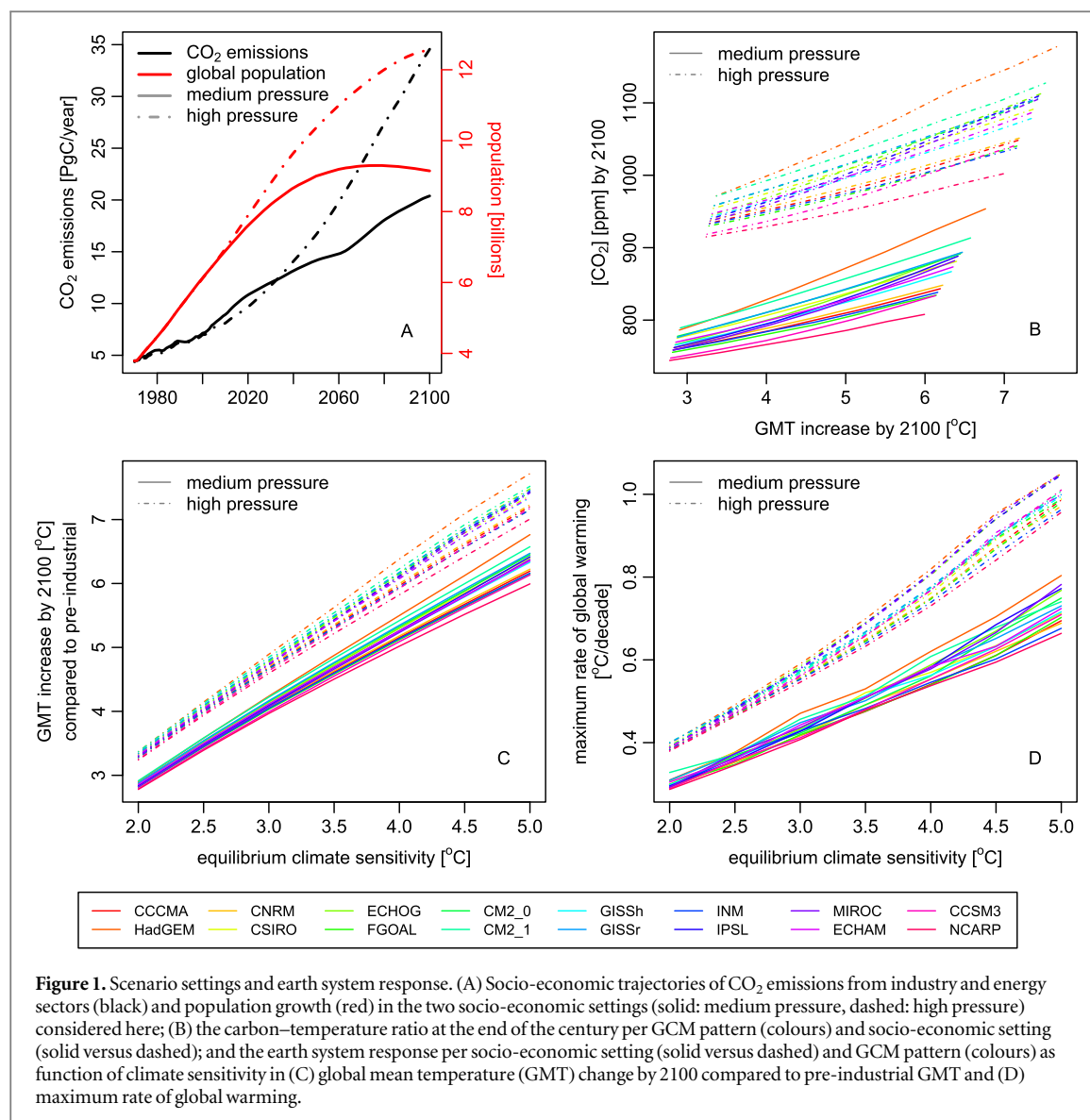
Methods

Study design

We study the robustness of the land biosphere carbon sink under different socio-economic pathways (population, anthropogenic GHG emissions, and gross domestic product (GDP) trajectories), climate sensitivities and climate change patterns, analyzing 224 different cases in total. We define carbon balance reversal as the transition of the land biosphere from an average net carbon sink to an average net carbon source within the 21st century (i.e. the time horizon of potential political action). As the time frame for such a transition (within the 21st century) is largely arbitrary and determined by the time frame for which the socio-economic scenarios are defined, we test all findings also for an alternative definition of the carbon balance reversal to assess their robustness. For this alternative definition, we also include all cases that have not reached the state of an average net carbon source within the 21st century but that display a significant negative trend in in their carbon balance over at least the last 20 years that would lead to a carbon balance reversal if extrapolated to the year 2120. All results presented here hold for both alternative definitions of the carbon balance reversal, although the exact values of thresholds and magnitudes vary slightly between the two definitions. The focus on the 21st century is, however, consistent with the current debate on climate policies and a carbon balance reversal in that time frame is therefore of political relevance.

We specifically investigate the role of key uncertainties in climate change by varying climate sensitivity, which was found to strongly influence the land carbon balance (Govindasamy *et al* 2005), from 2.0° to 5.0° in 0.5° steps and spatial patterns of climate change by employing climate change patterns of 16 general circulation models (GCMs). The IPCC reports the likely range for equilibrium climate sensitivity as 1.5 °C–4.5 °C (Flato *et al* 2013). However, a higher value cannot be ruled out (Tanaka *et al* 2009) and we therefore increased the range of climate sensitivity up to the point where all other elements (socio-economic setting, GCM pattern) become irrelevant for carbon balance reversal. To cover the range of likely future socio-economic developments, we here investigate a high pressure and a medium pressure scenario that differ in population growth trajectories, development in GDP per capita, greenhouse gas (GHG) emissions from energy and industry sectors as well as assumptions on agricultural intensity and demand for bioenergy. Changes in land-use patterns, climate, vegetation composition and the terrestrial carbon balance are computed internally by our coupled modelling framework. Again, the selection of scenarios is tailored to cover the range where the robustness of the terrestrial carbon balance is ambiguous. A sensitivity test revealed that the terrestrial carbon sink is robust under a low pressure scenario and we therefore did not explore this in more detail here. Given the multiple feedback mechanisms, we expect that climate sensitivity is an important but not the only determinant of a possible carbon balance reversal. The modelling setup allows for accounting for all dynamics of the terrestrial biosphere under changing agricultural productivity patterns and associated land-use change as well as dynamics of the natural vegetation (e.g. boreal greening) and carbon stocks.

Figure 1. Scenario settings and earth system response. (A) Socio-economic trajectories of CO_2 emissions from industry and energy sectors (black) and population growth (red) in the two socio-economic settings (solid: medium pressure, dashed: high pressure) considered here; (B) the carbon–temperature ratio at the end of the century per GCM pattern (colours) and socio-economic setting (solid versus dashed); and the earth system response per socio-economic setting (solid versus dashed) and GCM pattern (colours) as function of climate sensitivity in (C) global mean temperature (GMT) change by 2100 compared to pre-industrial GMT and (D) maximum rate of global warming.

The socio-economic scenarios on population growth and consumption and the resulting CO_2 emissions from industry and energy (figure 1(A)) largely determine future atmospheric CO_2 concentrations (dashed versus solid lines in figure 1(B)) and climate change (figure 1(C)), but there is substantial uncertainty in future atmospheric CO_2 concentrations originating from the spatial patterns of climate change and associated carbon dynamics in the terrestrial biosphere. Differences in global mean temperature (GMT) increase and rate of global warming (°C/decade, figure 1(D)) are determined mainly by the uncertainty in climate sensitivity (Shindell 2014) (*x*-axis in figures 1(C) and (D)) but also by the socio-economic scenario and the GCM patterns and associated feedbacks.

The integrated assessment model IMAGE

The IMAGE model is an integrated assessment model (Bouwman *et al* 2006, Stehfest *et al* 2014) used to study the trends and policy interventions in global environmental change, covering agricultural and energy

systems, climate, land-use, carbon and nutrient dynamics, and a wide range of impact indicators. IMAGE has been used to provide the IPCC's emission scenarios in SRES (Nakicenovic and Swart 2000), and the representative concentration pathways (RCPs) (van Vuuren *et al* 2012), and is also one of the five integrated assessment models used in the quantification of the shared socioeconomic pathways (Kriegler *et al* 2012), and is extensively used for climate policy assessments (den Elzen *et al* 2011).

Based on trends in demographic and economic development, the energy and agricultural modules of IMAGE calculate change in energy and agricultural consumption, production and trade. The resulting production of agricultural commodities, including crops, livestock and biofuels, are allocated spatially on a 30 min grid. All biophysical processes are calculated on this spatial resolution of 30 min.

The atmospheric composition and climate model in IMAGE is based on MAGICC 6.0 (Meinshausen *et al* 2011) and computes changes in GMT as the result

of (a) atmospheric concentrations of various GHGs, including carbon dioxide, methane, nitrous oxide and halocarbons, (b) aerosols that reduce the radiative forcing and (c) several model parameters, including the equilibrium climate sensitivity, which allows us to directly modify this parameter. Using a pattern scaling approach, i.e. a set of location and month specific parameters that describe the relationship of changes in local weather conditions with GMT, these computed changes in GMT are converted into spatially explicit fields of monthly mean temperature, monthly precipitation, monthly mean cloudiness and monthly number of rainy days (appendix figure S1). The patterns scaling parameter sets are derived from 16 different GCM projections (appendix table S1). The pattern scaling approach allows us to compare the effect of different spatial patterns of climate change, which is another key uncertainty in the response of the land biosphere to climate change.

Here, the earlier model in IMAGE to calculate carbon cycle and the distribution of natural vegetation, BIOME (Klein Goldewijk *et al* 1994) has been replaced by the dynamic vegetation model LPJmL. In the new IMAGE version 3.0 (Stehfest *et al* 2014), LPJmL is the standard module in IMAGE for carbon dynamics, crop modelling and natural vegetation distribution. As such, the carbon dynamics computed by LPJmL as affected by the computed changes in climate, atmospheric CO_2 concentrations, and land-use change directly affect the simulation of GMT.

The dynamic global vegetation and agriculture model LPJmL

LPJmL is a dynamic global vegetation, hydrology and crop growth model (Sitch *et al* 2003, Gerten *et al* 2004, Bondeau *et al* 2007) developed for global-scale analyses of the terrestrial carbon and water cycle dynamics as well as agricultural systems. For the carbon cycle, simulations are based on the detailed representation of underlying processes at daily time steps, including stomatal conductance, photosynthesis, phenology and respiration, while carbon allocation and vegetation dynamics (i.e. turnover, mortality, competition for water and light) of the nine plant functional types (2 herbaceous, 7 woody) are computed at annual time steps. Agricultural vegetation is represented by 12 crop functional types and managed grassland (Bondeau *et al* 2007). The representation of agricultural lands in LPJmL is used in this model set up to only compute the carbon dynamics under land-use change, CO_2 fertilization and climate change. Changes in agricultural productivity patterns are computed within IMAGE in this model setup. Natural fires are simulated at annual time steps as an important element in the carbon cycle and driver of vegetation dynamics. Plants on natural vegetation stands compete for light and water and their comparative advantages across the environmental gradients determine the vegetation composition

dynamically. Plant tissue turnover is parameterized at fixed rates, but competition, growth efficiency and heat stress can increase mortality rates. Establishment of new saplings is controlled by bio-climatic limits. Dead biomass is passed on to the litter layers where it decomposes to form soil carbon stocks and releases CO_2 to the atmosphere. Carbon from heterotrophic respiration of the litter and soil carbon pools and carbon from burnt biomass is returned to the atmosphere as CO_2. Climate and soil conditions are assumed to be homogeneous per grid cell (30 min × 30 min longitude, latitude) but each grid cell can consist of one natural stand and multiple agricultural stands with annually varying shares (Bondeau *et al* 2007). Crops and grassland on agricultural stands do not compete for water with other stands but have their own water budgets. Land-use change between natural land, cropland and managed grassland is simulated at annual time steps. The ability of LPJmL to reproduce observed dynamics of the terrestrial carbon cycle and vegetation patterns has been demonstrated against various data products, including eddy flux tower measurements (Jung *et al* 2008, Luyssaert *et al* 2010), satellite observations of phenology (Lucht *et al* 2002), vegetation (Cramer *et al* 2001, Hickler *et al* 2006) and fire patterns (Thonicke *et al* 2001), and free air carbon enrichment experiments (Gerten *et al* 2005). Carbon and water cycles are fully coupled in LPJmL simulations and the validation of water flux components against river gauge data (Biemans *et al* 2009) and evapotranspiration (Gerten *et al* 2005) is an additional validation of the underlying plant and soil processes implemented in LPJmL. In comparison to other DGVMs, LPJmL is of relatively high complexity and carbon cycle estimates are well within the range of other dynamic global vegetation models, as compared in the Intersectoral Impact Model Intercomparison (ISI-MIP) (Friend *et al* 2014).

Model coupling

In the coupling between LPJmL and IMAGE, operating fully dynamically coupled at annual time-steps, all annual land-use and monthly climate data fields (30 min × 30 min grid) as well as global $[CO_2]$ values are provided from IMAGE to LPJmL. LPJmL computes daily weather variables from these monthly values with an internal weather generator that is also used in standard stand-alone applications of LPJmL (Gerten *et al* 2004). LPJmL provides IMAGE with the complete set of carbon pools and fluxes for its climate and land use model (appendix table S2). We add inter-annual variability from the CRU 2.0 monthly climatology (New *et al* 2000) to the smooth 30-year climate data, which is calculated based on the simple climate model MAGICC6 (Meinshausen *et al* 2011) within IMAGE. When applying the extracted 30-year time series of CRU variability to the years 2001–2100, the annual sequence was re-ordered randomly.

For the coupling with IMAGE, LPJmL has been modified to allow for timber harvest and turnover and decay of timber and timber products. Timber harvest is driven by the total demand per region for sawlogs, pulp/paper wood and fuelwood. Production and trade assumptions for saw logs and paper/pulp wood are adopted from external models/scenarios, such as EFI-GTM (Kallio *et al* 2004). Demand for fuelwood is computed internally in IMAGE, based on the TIMER model assuming that not all timber is produced from formal forestry activities, but part is also collected from non-forest areas, such as thinning orchards and along roadsides (FAO 2001, 2008). The land-use change mechanisms of IMAGE internally determine which grid-cells are used for timber harvest (Stehfest *et al* 2014). Timber harvest is implemented as clear cut on the first day of the year, when all land use fractions are updated from IMAGE. Timber demand and land-use change is computed every five years by IMAGE and land fractions per pixel are passed on to LPJmL. Agricultural land use can occupy any fraction of land per grid cell, timber harvest always clears the entire fraction of that grid cell that is occupied by natural vegetation. As there is no specific forestry land use type implemented in LPJmL, timber harvest removes tree biomass from natural vegetation. After timber harvest, land can be used for agricultural production or natural vegetation can regrow. Repeated timber harvest events must allow at least 30 years of regrowth.

If the land is not used for agricultural production after timber harvest, saplings establish in the next year as for natural vegetation (Sitch *et al* 2003). After harvest, all above ground woody parts (hard wood, 2/3 of sapwood) are transferred to two timber product pools based on fractions supplied by IMAGE. Remaining biomass from deforested plot (leaves, roots, 1/3 of sapwood) is transferred to the litter pools just as litter fall from mortality and turnover in natural vegetation. The two timber product pools represent different wood product classes with fast (10 years) and slow (100 years) turnover rates, respectively and are initialized following Lauk *et al* (2012).

To simulate the carbon dynamics of different land-use systems, the 19 different agricultural production types in IMAGE have been mapped to the 12 crops and the managed grassland system as implemented in LPJmL (Bondeau *et al* 2007, Lapola *et al* 2009), see appendix table S3.

Scenario assumptions

In the scenarios analyzed we combine two consistent socio-economic scenarios high pressure (Nakicenovic and Swart 2000) and medium pressure (van Vuuren *et al* 2010) with stratified scenarios on equilibrium climate sensitivity (seven sets with climate sensitivities ranging from 2.0° to 5.0° in 0.5° intervals) and patterns of climate change derived from 16 GCM simulations (extended data table S3). While climate sensitivity is typically used as a GCM-specific parameter in the climate model MAGICC, we here use an average parameterization for MAGICC across all GCM patterns and only vary climate sensitivity according to the scenario. We acknowledge that this causes some inconsistency between GCM pattern and equilibrium climate sensitivity, but this is the only way to systematically test the uncertainty in both dimensions. The socio-economic scenario assumptions are drawn from different scenario families (SRES and RCP), yet as the scenario assumptions used here only comprise growth in population, and wealth (GDP per capita), GHG emissions from the industry and energy sectors as well as assumptions on agricultural intensity and demand for bioenergy, these scenarios are perfectly comparable as all changes in land-use, climate and carbon cycle dynamics (including ocean uptake) are computed consistently. We also tested a low pressure scenario (van Vuuren *et al* 2011) to see if there is any likelihood for carbon reversal under a low emission scenario. We thus only tested the GCM pattern which showed the largest likelihood for carbon reversal (HadGEM) for the high and medium pressure scenarios and one that showed relatively low likelihood for carbon reversal (CCCMA). At all climate sensitivities tested here, these 2 GCM patterns never lead to a carbon balance reversal.

Results: mechanisms and patterns of carbon balance reversal

We find that the land biosphere's carbon balance can be reversed under both socio-economic scenarios (medium and high pressure) and at any equilibrium climate sensitivity of 2.5 °C or above and for any of the 16 GCM climate pattern studied here. However, under the medium pressure scenario, the land biosphere carbon sink can be maintained for climate sensitivities of up to 5.0 °C for some GCM patterns. For some socio-economic settings and GCM patterns, the land biosphere carbon sink can tolerate increases in GMT up to 6 °C above pre-industrial temperatures by 2100. Depending on the sensitivity to the scenario settings and the corresponding feedback strengths, the annual net carbon exchange rates between atmosphere and the land biosphere range between -10.1 (source) and 4.5 Pg C yr^{-1} (sink) (figure 2), and a carbon balance reversal (transition from terrestrial net carbon uptake to net carbon release) can occur as early as 2030. A sensitivity test with two extreme GCM patterns (HadGEM and CCCMA) with a strong climate mitigation scenario (low pressure), showed that the terrestrial carbon sink is robust under these conditions (green lines in figure 2, appendix figure S2).

Cumulative 21st century carbon exchange between the land biosphere and atmosphere can range between a net carbon sequestration of 330 Pg C and a net release of 340 Pg C to the atmosphere (appendix figure S3), and atmospheric CO_2 concentrations can
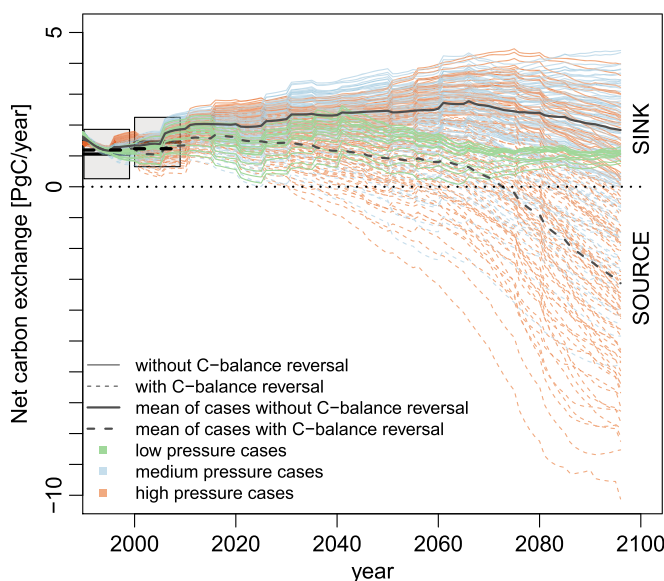
Figure 2. 10-year moving average net carbon exchange rates between the land biosphere and the atmosphere. Negative values indicate a net release of carbon to the atmosphere. Grey boxes in the 1990s and 2000s show observational net carbon exchange rates (Le Quéré et al 2014), which can be reproduced well by the coupled models (dashed lines in the grey boxes indicate the simulated mean). We show 10-year moving average values because land-use change is implemented at 5-yearly time steps only. We only tested the GCM pattern which showed the largest likelihood for carbon balance reversal (HadGEM) and one that showed relatively low likelihood (CCCMA) with a low pressure scenario (green lines). At all climate sensitivities tested here, these 2 GCM patterns never lead to a carbon balance reversal under the low emission scenario.
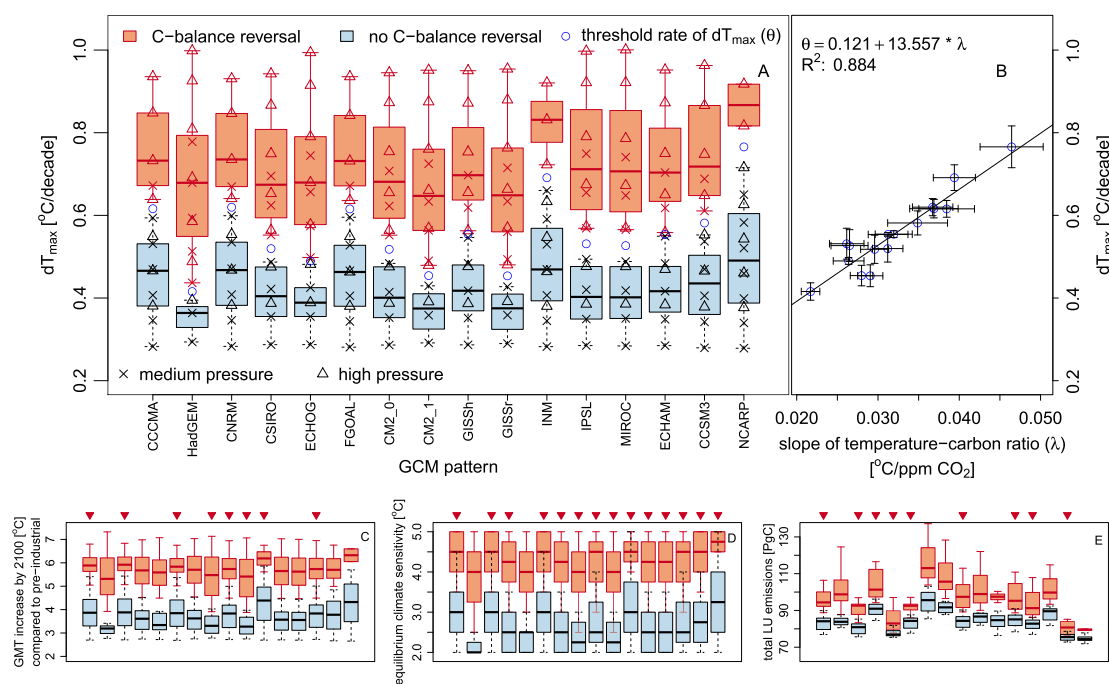

Figure 3. The reversal of the terrestrial carbon balance is also related to the maximum rate of global warming (A) and the slope of the GCM-pattern specific temperature–carbon ratio λ (B). The y-axis is the same in panels A and B. A clear maximal rate of global warming threshold can be identified between 0.41 and 0.76 °C/decade. Generally, the land biosphere's carbon balance is reversed at higher GMT (C), climate sensitivity (D) and land-use (LU) emissions (E) but there is no clear threshold for the carbon balance reversal. For better visibility, red marks above panels C–E indicate GCM patterns where the range of GMT (C), climate sensitivity (D) or LU emissions (E) of the cases with carbon balance reversal (red whiskers) overlap with the cases without carbon balance reversal (blue whiskers). Bars display the interquartile range of values; whiskers extend to the full range of values covered. Individual simulations are indicated with crosses (medium pressure) or triangles (high pressure) in panel A.

vary between 915 and 1180 (high pressure scenario) and 744 and 954 (medium pressure scenario) ppm by 2100 (figure 1(B)). Reflecting the large differences in [CO$_2$] and GMT (2.7–7.7 above pre-industrial by 2100), ocean uptake ranges between 1.3 and 7.3 Pg C yr^{-1} (appendix figure S4).

We find that the maximum rate of global warming (dT_{max}, maximal increase in GMT per decade) allows a clear distinction between cases that lead to a reversal of the terrestrial carbon balance in the 21st century and those that do not (figure 3(A), appendix figure S5). A threshold rate (θ) separating the cases is defined as the mean of the lowest dT_{max} of cases that lead to carbon balance reversal and the highest dT_{max} of cases that show a robust terrestrial carbon sink (open circles in figures 3(A) and (B)). This threshold rate is specific to each GCM pattern and ranges between 0.41 and 0.76 °C/decade. In the settings studied here, rates of global warming typically increase over time so that the maximum rate of global warming represents the rate of global warming in the decade 2091–2100 in most cases (appendix figure S6). The threshold θ is strongly related to the slope of the temperature–carbon ratio (λ, figures 1(B) and 3(B)) that describes the linear relationship of end-of-21st-century GMT and end-of-21st-century [CO_2]. This slope (λ) is mainly determined by the GCM pattern, but there is some uncertainty from the socio-economic scenario (solid versus dashed lines in figure 1(B)), which is represented as horizontal error bars in figure 3(B). Results show that large λ (i.e. strong rise in GMT per ppm [CO_2]) are correlated with high threshold rates of warming (θ). This, however, does not offer an underlying explanatory mechanism, but simply describes the complex coupling of the land biosphere carbon balance and global warming: if transient increases in GMT per ppm [CO_2] is low (low λ), there is a strong response in [CO_2] to increases in GMT (inverse of λ). Consequently, a land biosphere carbon reversal can occur at relatively low increases in GMT and related low dT_{max} (appendix figure S7). It has to be noted that dT_{max} is not the cause of the carbon balance reversal, but an indicator of relevant dynamic interactions, as maximum dT typically occur at the end of the century, while the reversal itself can occur as early as 2030.

There is some overlap (red marks in figure 3) in GMT increase (figure 3(C)), equilibrium climate sensitivity (figure 3(D)) and total land-use emissions (figure 3(E)) between the cases leading to and those without a reversal of the terrestrial carbon balance, so that no threshold can be identified for these indicators.

In accordance with previous studies, we find that the carbon balance reversal becomes more likely with rising GMT and equilibrium climate sensitivity (Govindasamy *et al* 2005) or land-use emissions (figures 3(C)–(E), appendix figure S5). However, the robustness of the land carbon sink is not clearly determined by these parameters. Reversal of the land carbon balance is possible but not inevitable for equilibrium climate sensitivities between 2.5 °C and 5.0 °C, for GMT increase by 2100 between 3.9 °C and 5.9 °C above pre-industrial, and with carbon emissions from land-use change between 76 and 103 Pg C. Below these ranges, none of the 224 cases analyzed here leads to a terrestrial carbon balance reversal by
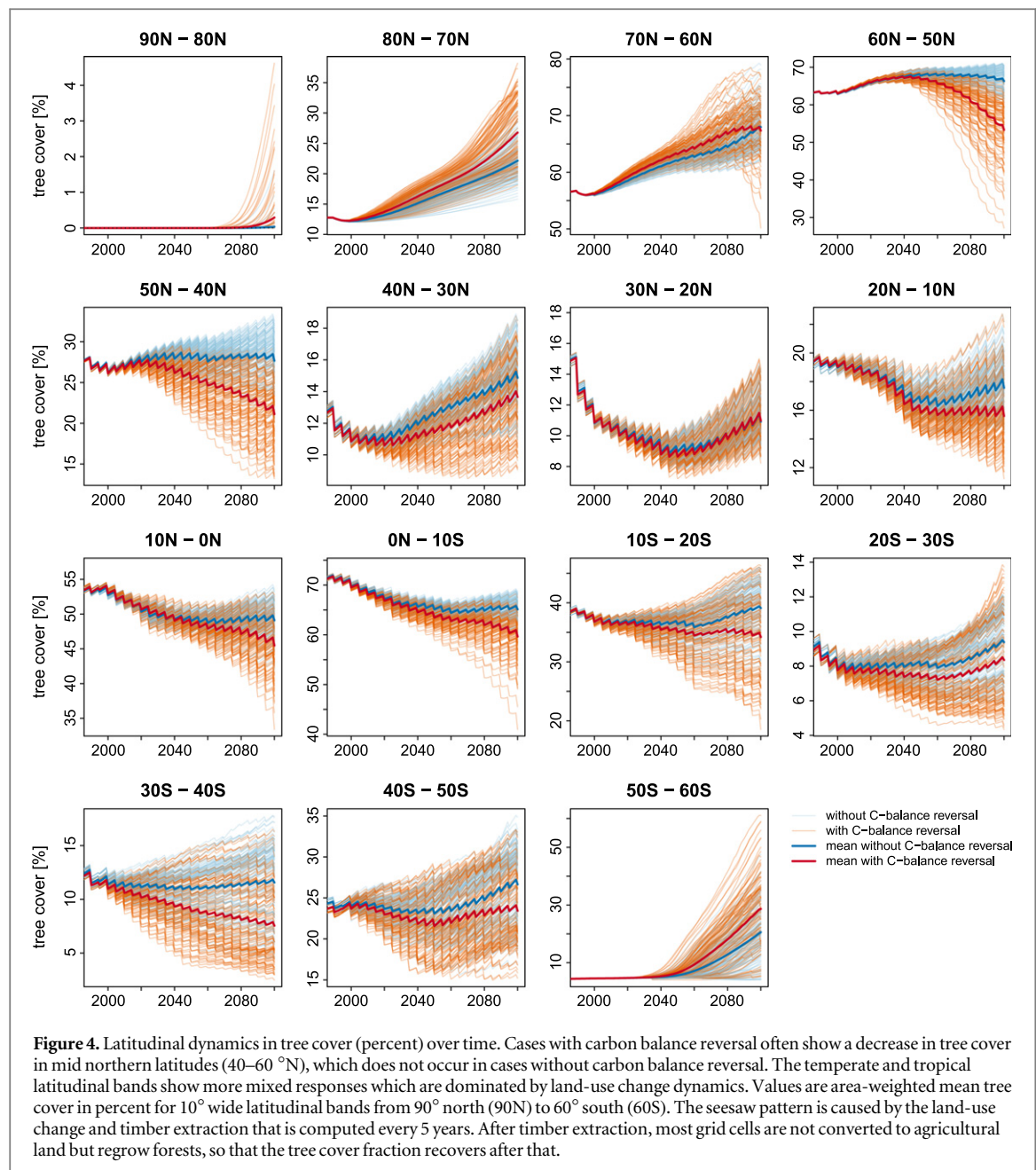
2100 (the time at which the scenarios end). As with dT_{max}, the spatial pattern of climate change is an important modifier of the possible range of GMT increase, land-use change carbon emissions and climate sensitivities within which the land biosphere carbon sink is robust.

Spatial analysis reveals that the most important underlying mechanisms are a change in vegetation patterns that leads to a decline in tree cover and more pronounced soil carbon losses in the high northern latitudes. The release of carbon from tree cover decline is most prominent in the mid latitudes (40–60 °N, figures 4 and 5). Heat and drought stress affecting plant productivity, tissue mortality, sapling survival and fire frequency lead to regionally decreasing tree density (Allen *et al* 2010, Park Williams *et al* 2013, McDowell and Allen 2015), which extends further into the boreal forests under climate change (appendix figure S8). The changes in tree cover of temperate and tropical regions are mainly driven by land-use change. The increasing tree cover in the high latitudes (>60 °N) cannot compensate for the carbon losses in regions with higher carbon densities. The high latitudes (>60 °N) are largely subject to losses in soil carbon in all cases, but this loss is more pronounced (∼30 kg C m^{-2} more in most regions) in the cases of carbon balance reversal, which generally have lower soil carbon contents than the cases without carbon balance reversal. The only exception is the area of strong tree cover decline under carbon balance reversal, where increased tree mortality leads to larger inputs of organic matter into the litter and soil pools (appendix figure S9). In combination, the regions of tree cover decline and more pronounced losses in soil carbon, which are predominantly in the boreal zone, constitute the regional hotspots of terrestrial carbon balance reversal.

Discussion: implications for Earth system research

Our analysis confirms the rising likelihood of a positive land–atmosphere carbon feedback with rising GMT in a framework that accounts for the multiple feedbacks of terrestrial carbon balance, atmospheric CO_2 concentrations, ocean uptake, climate change and land-use patterns, all influencing each other. Only at climate sensitivities above 4.5° there is high probability ($p = 0.88$) of a terrestrial carbon balance reversal and for equilibrium climate sensitivities of 2.0° or below, the terrestrial carbon balance is robust against variations in population growth and GHG emissions and the associated changes in land use and climate change as covered by the analyzed set of cases (appendix figure S10).
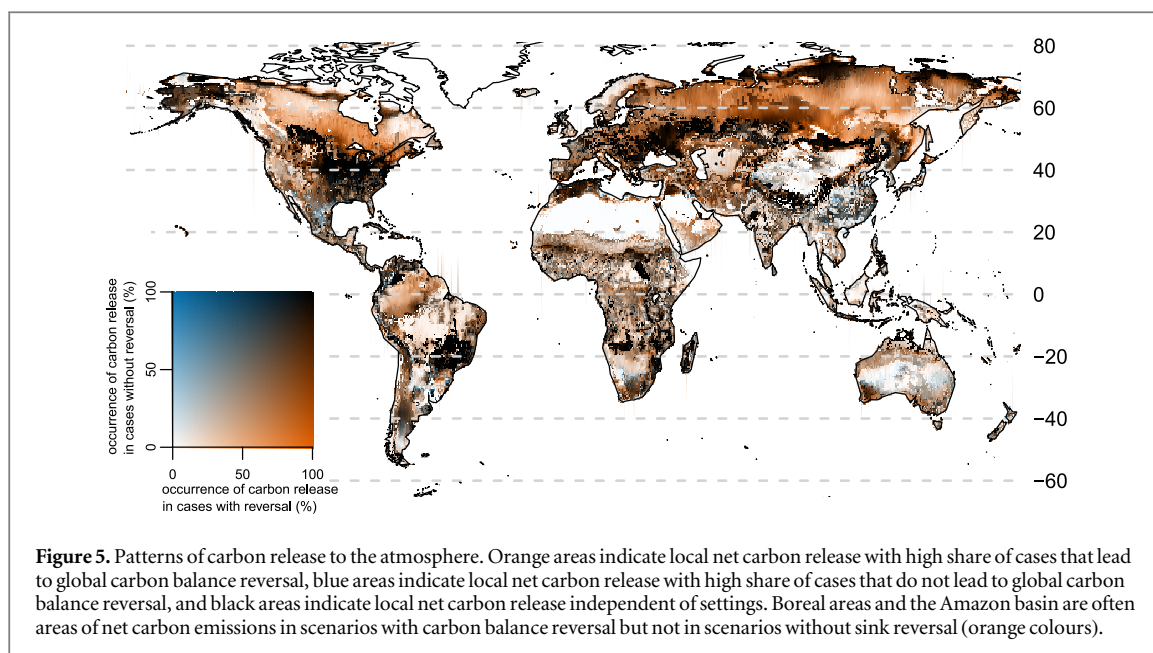
The analysis conducted here covers the relevant feedback mechanisms between the terrestrial carbon balance, atmospheric CO_2 concentrations, climate

Figure 4. Latitudinal dynamics in tree cover (percent) over time. Cases with carbon balance reversal often show a decrease in tree cover in mid northern latitudes (40–60 °N), which does not occur in cases without carbon balance reversal. The temperate and tropical latitudinal bands show more mixed responses which are dominated by land-use change dynamics. Values are area-weighted mean tree cover in percent for 10° wide latitudinal bands from 90° north (90N) to 60° south (60S). The seesaw pattern is caused by the land-use change and timber extraction that is computed every 5 years. After timber extraction, most grid cells are not converted to agricultural land but regrow forests, so that the tree cover fraction recovers after that.

change, land productivity, and land-use change. We do not cover, however, the substantial uncertainty in land carbon dynamics as simulated by various global vegetation models (Friend *et al* 2014). Besides the much debated uncertainty in the effects of CO_2 fertilization on the terrestrial carbon balance (Friedlingstein *et al* 2006, Fatichi *et al* 2014, Schimel *et al* 2015), the uncertainty in carbon cycle simulations from global vegetation models is also rooted in the processes that control the carbon back-flux from the land biosphere to the atmosphere, such as plant mortality, tissue turnover and fire dynamics (Friend *et al* 2014), where substantially more research is required for better model evaluation and improvement. Multi-sectoral DGVM intercomparisons have shown that the LPJmL is not an outlier with respect to projected changes in NPP (Sitch *et al* 2008, Friend *et al* 2014) and overall magnitude of

biogeochemical shifts under climate change (Warszawski *et al* 2013), but that simulated carbon residence time in vegetation declines more strongly under global warming than in other models, i.e. due to processes such as heat stress on boreal vegetation that are not taken into account in other models (Friend *et al* 2014). The decline in vegetation carbon in the mid northern latitudes, which is a relevant driver of change in our study (figures 4 and 5), is also simulated by HYBRID4 and LPJmL in the ISI-MIP biome sector model intercomparison (Friend *et al* 2014) that both simulate changes in vegetation composition.

Forests have been identified as important carbon sinks (Pan *et al* 2011) and simulating their dynamics under climate change is essential for assessing future carbon dynamics but subject to uncertainty in model design and parametrization (Fisher *et al* 2014, Medlyn

Figure 5. Patterns of carbon release to the atmosphere. Orange areas indicate local net carbon release with high share of cases that lead to global carbon balance reversal, blue areas indicate local net carbon release with high share of cases that do not lead to global carbon balance reversal, and black areas indicate local net carbon release independent of settings. Boreal areas and the Amazon basin are often areas of net carbon emissions in scenarios with carbon balance reversal but not in scenarios without sink reversal (orange colours).

et al 2015). While the increasing risk of a carbon balance reversal with rising GMT has been studied, we here identify the key region that determines the carbon balance reversal, the boreal zone, and find that changes in tree cover in the temperate and tropical zones are more mixed and mainly driven by land-use change. The strong relationship with declining tree cover in mid to high northern latitudes (figure 4) suggests that the carbon balance reversal is particularly affected by biosphere processes, namely vegetation dynamics and related underlying processes such as mortality rates and tissue turnover that determine the competitiveness of species (or plant functional types, which are typically used to aggregate species in simulations) (Friend *et al* 2014). This central element of the terrestrial carbon cycle can only be captured by models that dynamically simulate vegetation composition (Warszawski *et al* 2013), and needs to be analyzed also with respect to the aggregated representation of plant species, which can greatly affect carbon cycle simulations (Alton 2011) and vegetation composition (Midgley *et al* 2010, Yu and Gao 2011, Song and Zeng 2014).

The rate of global warming is not the most prominent measure for characterizing climate change, but it affects natural and socio-economic systems by constraining the time required to adjust to changes by e.g. migration (Kirschbaum 2014). Our results show that it serves well as an indicator for the global carbon balance not only as the derivative of GMT but also as a factor in vegetation mechanisms.

Terrestrial carbon balance reversal can occur as early as 2030 (in the most extreme case, see figure 2), a short time frame for implementing climate mitigation measures. A reversed carbon balance would strongly complicate a stabilization of atmospheric CO_2 concentrations. A loss of the terrestrial carbon sink would imply that climate change is amplified unless

anthropogenic emissions are strongly reduced below conventional mitigation efforts to compensate for the missing carbon sequestration of currently 1.3 Pg C yr^{-1} (Le Quéré *et al* 2014) and to counterbalance additional emissions of up to 10.1 Pg C yr^{-1} (figure 2). The land biosphere has the potential to absorb or to release about 300 Pg C over the remaining 21st century, which is approximately one third of the remaining emission budget for the 2-degree target (Meinshausen *et al* 2009, IPCC 2013), although this estimate of a total allowable emission budget to stay under the 2-degree target includes some land biosphere carbon cycle response that is computed in the underlying earth system model simulations (IPCC 2013).

The range of settings under which a carbon balance reversal can occur is broad, including socio-economic pathways with high as well as moderate population and GHG emission levels, rates of global warming between 0.41 and 1.0 °C/decade, equilibrium climate sensitivities of 2.5 °C upwards, and increases in agricultural area between 0.5 and 6.2 million hectares. The lower ends of these estimates, within given uncertainty, are ample reason for concern, as they demonstrate that a reversal of the land biosphere carbon balance is not only a probability in high-end scenarios but with current uncertainties in parameter estimates and modelling abilities already possible under moderate global change. This is strongly dependent on the spatial patterns of climate change, as demonstrated here by employing a patterns scaling approach that allows for direct comparability of different GCM-specific patterns of change under the same climate sensitivities and food demand trajectories. A clearer understanding of the vegetation mechanisms that strongly affect the terrestrial carbon balance would help to reduce uncertainty in carbon cycle models (Meinshausen *et al* 2011, Friend

et al 2014) and thus help to narrow down the uncertainty of tolerable cumulative CO_2 emissions (IPCC 2013).

Acknowledgments

References

Allen C D *et al* 2010 A global overview of drought and heat-induced tree mortality reveals emerging climate change risks for forests *For. Ecol. Manag.* **259** 660–84

Alton P B 2011 How useful are plant functional types in global simulations of the carbon, water, and energy cycles? *J. Geophys. Res.: Biogeosci.* **116** G01030

Arora V K *et al* 2013 Carbon-concentration and carbon-climate feedbacks in CMIP5 Earth system models *J. Clim.* **26** 5289–314

Biemans H, Hutjes R W A, Kabat P, Strengers B J, Gerten D and Rost S 2009 Effects of precipitation uncertainty on discharge calculations for main river basins *J. Hydrometeorol.* **10** 1011–25

Bondeau A *et al* 2007 Modelling the role of agriculture for the 20th century global terrestrial carbon balance *Glob. Change Biol.* **13** 679–706

Bouwman A, Kram T and Klein Goldewijk K 2006 *Integrated Modelling of Global Environmental Change: An overview of IMAGE 2.4* (The Hague, The Netherlands: PBL Netherlands Environmental Assessment Agency)

Cramer W *et al* 2001 Global response of terrestrial ecosystem structure and function to CO_2 and climate change: results from six dynamic global vegetation models *Glob. Change Biol.* **7** 357–73

den Elzen M G J, Hof A F, Mendoza Beltran A, Grassi G, Roelfsema M, van Ruijven B, van Vliet J and van Vuuren D P 2011 The copenhagen accord: abatement costs and carbon prices resulting from the submissions *Environ. Sci. Policy* **14** 28–39

FAO 2001 Plantations and wood energy *Report based on the work of DJ Mead Forest Plantation Thematic Papers, Working Paper 5* (Rome: Forest Resources Development Service, Forest Resources Division, FAO)

FAO 2008 Forests and energy, key issues *FAO Forestry Paper 154* (Rome, Italy: Food and Agriculture Organization of the United Nations)

Fatichi S, Leuzinger S and Körner C 2014 Moving beyond photosynthesis: from carbon source to sink-driven vegetation modeling *New Phytol.* **201** 1086–95

Fisher J B, Huntzinger D N, Schwalm C R and Sitch S 2014 Modeling the terrestrial biosphere *Ann. Rev. Environ. Resour.* **39** 91–123

Flato G *et al* 2013 Climate change 2013: the physical science basis *Contribution of Working Group I to the Fifth Assessment Report of the Intergovernmental Panel on Climate Change* ed T F Stocker *et al* (Cambridge: Cambridge University Press)

Friedlingstein P *et al* 2006 Climate-carbon cycle feedback analysis, results from the C^{4}MIP model intercomparison *J. Clim.* **19** 3337–53

Friend A D *et al* 2014 Carbon residence time dominates uncertainty in terrestrial vegetation responses to future climate and atmospheric CO_2 *Proc. Natl Acad. Sci. USA* **111** 3280–5

Gasser T and Ciais P 2013 A theoretical framework for the net land-to-atmosphere CO_2 flux and its implications in the definition of 'emissions from land-use change' *Earth Syst. Dyn.* **4** 171–86

Gatti L V *et al* 2014 Drought sensitivity of amazonian carbon balance revealed by atmospheric measurements *Nature* **506** 76–80

Gerten D, Lucht W, Schaphoff S, Cramer W, Hickler T and Wagner W 2005 Hydrologic resilience of the terrestrial biosphere *Geophys. Res. Lett.* **32**

Gerten D, Schaphoff S, Haberlandt U, Lucht W and Sitch S 2004 Terrestrial vegetation and water balance - hydrological evaluation of a dynamic global vegetation model *J. Hydrol.* **286** 249–70

Govindasamy B, Thompson S, Mirin A, Wickett M, Caldeira K and Delire C 2005 Increase of carbon cycle feedback with climate sensitivity: results from a coupled climate and carbon cycle model *Tellus* B **57** 153–63

Haberl H, Erb K H, Krausmann F, Gaube V, Bondeau A, Plutzar C, Gingrich S, Lucht W and Fischer-Kowalski M 2007 Quantifying and mapping the human appropriation of net primary production in earth's terrestrial ecosystems *Proc. Natl Acad. Sci. USA* **104** 12942–7

Hickler T, Prentice I C, Smith B, Sykes M T and Zaehle S 2006 Implementing plant hydraulic architecture within the LPJ dynamic global vegetation model *Glob. Ecol. Biogeogr.* **15** 567–77

IPCC 2013 Climate change 2013: the physical science basis *Contribution of Working Group I to the Fifth Assessment Report of the Intergovernmental Panel on Climate Change* ed T F Stocker *et al* (Cambridge: Cambridge University Press)

Jung M, Verstraete M, Gobron N, Reichstein M, Papale D, Bondeau A, Robustelli M and Pinty B 2008 Diagnostic assessment of European gross primary production *Glob. Change Biol.* **14** 2349–64

Kallio A, Moiseyev A and Solberg B 2004 The global forest sector model EFIGTM—the model structure *Technical Report* 15, E F Institute, Joensuu, Finland

Kicklighter D W, Cai Y, Zhuang Q, Parfenova E I, Paltsev S, Sokolov A P, Melillo J M, Reilly J M, Tchebakova N M and Lu X 2014 Potential influence of climate-induced vegetation shifts on future land use and associated land carbon fluxes in Northern Eurasia *Environ. Res. Lett.* **9** 035004

Kirschbaum M U F 2014 Climate-change impact potentials as an alternative to global warming potentials *Environ. Res. Lett.* **9** 034014

Klein Goldewijk K, Minnen J V, Kreileman G, Vloedbeld M and Leemans R 1994 Simulating the carbon flux between the terrestrial environment and the atmosphere *Water Air Soil Pollut.* **76** 199–230

Kriegler E, O'Neill B C, Hallegatte S, Kram T, Lempert R J, Moss R H and Wilbanks T 2012 The need for and use of socio-economic scenarios for climate change analysis: a new approach based on shared socio-economic pathways *Glob. Environ. Change* **22** 807–22

Lapola D M, Priess J A and Bondeau A 2009 Modeling the land requirements and potential productivity of sugarcane and jatropha in Brazil and India using the LPJmL dynamic global vegetation model *Biomass Bioenergy* **33** 1087–95

Lauk C, Haberl H, Erb K-H, Gingrich S and Krausmann F 2012 Global socioeconomic carbon stocks in long-lived products 1900–2008 *Environ. Res. Lett.* **7** 034023

Le Quéré C *et al* 2014 Global carbon budget 2013 *Earth Syst. Sci. Data* **6** 235–63

Lucht W, Prentice I C, Myneni R B, Sitch S, Friedlingstein P, Cramer W, Bousquet P, Buermann W and Smith B 2002 Climatic control of the high-latitude vegetation greening trend and pinatubo effect *Science* **296** 1687–9

Luyssaert S *et al* 2010 The European carbon balance: III. Forests *Glob. Change Biol.* **16** 1429–50

McDowell N G and Allen C D 2015 Darcy's law predicts widespread forest mortality under climate warming *Nat. Clim. Change* **5** 669–72

Medlyn B E *et al* 2015 Using ecosystem experiments to improve vegetation models *Nat. Clim. Change* **5** 528–34

Meinshausen M, Meinshausen N, Hare W, Raper S C B, Frieler K, Knutti R, Frame D J and Allen M R 2009 Greenhouse-gas emission targets for limiting global warming to 2 °C *Nature* **458** 1158–62

Meinshausen M, Raper S C B and Wigley T M L 2011 Emulating coupled atmosphere–ocean and carbon cycle models with a simpler model, MAGICC6: I. Model description and calibration *Atmos. Chem. Phys.* **11** 1417–56

Midgley G F, Davies I D, Albert C H, Altwegg R, Hannah L, Hughes G O, O'Halloran L R, Seo C, Thorne J H and Thuiller W 2010 BioMove—an integrated platform simulating the dynamic response of species to environmental change *Ecography* **33** 612–6

Müller C, Eickhout B, Zaehle S, Bondeau A, Cramer W and Lucht W 2007 Effects of changes in CO_2, climate, and land use on the carbon balance of the land biosphere during the 21st century *J. Geophys. Res.—Biogeosci.* **112** G02032

Nakicenovic N and Swart R 2000 *Special Report on Emission Scenarios* (Cambrige: Cambridge University Press)

Nelson G C *et al* 2014 Climate change effects on agriculture: economic responses to biophysical shocks *Proc. Natl Acad. Sci. USA* **111** 3274–9

New M G, Hulme M and Jones P D 2000 Representing twentieth-century space-time climate variability: II. Development of 1901–1996 monthly grids of terrestrial surface climate *J. Clim.* **13** 2217–38

Pan Y *et al* 2011 A large and persistent carbon sink in the world's forests *Science* **333** 988–93

Park Williams A *et al* 2013 Temperature as a potent driver of regional forest drought stress and tree mortality *Nat. Clim. Change* **3** 292–7

Pongratz J, Reick C H, Houghton R A and House J 2013 Terminology as a key uncertainty in net land use flux estimates *Earth Syst. Dyn. Discuss.* **4** 677–716

Poulter B *et al* 2014 Contribution of semi-arid ecosystems to interannual variability of the global carbon cycle *Nature* **509** 600–3

Rosenzweig C *et al* 2014 Assessing agricultural risks of climate change in the 21st century in a global gridded crop model intercomparison *Proc. Natl Acad. Sci. USA* **111** 3268–73

Schaphoff S, Lucht W, Gerten D, Sitch S, Cramer W and Prentice I C 2006 Terrestrial biosphere carbon storage under alternative climate projections *Clim. Change* **74** 97–122

Scheffer M, Brovkin V and Cox P M 2006 Positive feedback between global warming and atmospheric CO_2 concentrations inferred from past climate change *Geophys. Res. Lett.* **33** L10702

Schimel D, Stephens B B and Fisher J B 2015 Effect of increasing CO_2 on the terrestrial carbon cycle *Proc. Natl Acad. Sci. USA* **112** 436–41

Schmitz C *et al* 2014 Land-use change trajectories up to 2050: insights from a global agro-economic model comparison *Agric. Econ.* **45** 69–84

Schwalm C R, Williams C A, Schaefer K, Baldocchi D, Black T A, Goldstein A H, Law B E, Oechel W C, Paw U K T and Scott R L 2012 Reduction in carbon uptake during turn of the century drought in western North America *Nat. Geosci.* **5** 551–6

Shindell D T 2014 Inhomogeneous forcing and transient climate sensitivity *Nat. Clim. Change* **4** 274–7

Sitch S *et al* 2003 Evaluation of ecosystem dynamics, plant geography and terrestrial carbon cycling in the LPJ dynamic global vegetation model *Glob. Change Biol.* **9** 161–85

Sitch S *et al* 2008 Evaluation of the terrestrial carbon cycle, future plant geography and climate-carbon cycle feedbacks using five dynamic global vegetation models (DGVMs) *Glob. Change Biol.* **14** 2015–39

Song X and Zeng X D 2014 Investigation of uncertainties of establishment schemes in dynamic global vegetation models *Adv. Atmos. Sci.* **31** 85–94

Stehfest E *et al* 2014 *Integrated Assessment of Global Environmental Change with Image 3.0. Model Description and Policy Applications* (The Hague, The Netherlands: PBL Netherlands Environmental Assessment Agency)

Tanaka K, Raddatz T, O'Neill B C and Reick C H 2009 Insufficient forcing uncertainty underestimates the risk of high climate sensitivity *Geophys. Res. Lett.* **36** L16709

Thonicke K, Venevsky S, Sitch S and Cramer W 2001 The role of fire disturbance for global vegetation dynamics: coupling fire into a dynamic global vegetation model *Glob. Ecol. Biogeogr.* **10** 661–77

van Vuuren D P, Stehfest E, den Elzen M G J, van Vliet J and Isaac M 2010 Exploring IMAGE model scenarios that keep greenhouse gas radiative forcing below 3 W m^{-2} in 2100 *Energy Econ.* **32** 1105–20

van Vuuren D *et al* 2011 RCP2.6: exploring the possibility to keep global mean temperature increase below 2 °C *Clim. Change* **109** 95–116

van Vuuren D P *et al* 2012 A proposal for a new scenario framework to support research and assessment in different climate research communities *Glob. Environ. Change* **22** 21–35

Warszawski L *et al* 2013 A multi-model analysis of risk of ecosystem shifts under climate change *Environ. Res. Lett.* **8** 044018

Yu M and Gao Q O 2011 Leaf-traits and growth allometry explain competition and differences in response to climatic change in a temperate forest landscape: a simulation study *Ann. Bot.* **108** 885–94